Cite this: *Nanoscale*, 2011, **3**, 1910

www.rsc.org/nanoscale

PAPER

Synthesis of recrystallized anatase TiO_2 mesocrystals with Wulff shape assisted by oriented attachment†

Rafael O. Da Silva,[a] Ricardo H. Gonçalves,[a] Daniel G. Stroppa,[bc] Antonio J. Ramirez[b] and Edson R. Leite*[a]

Received 22nd December 2010, Accepted 16th February 2011
DOI: 10.1039/c0nr01016b

In this work, we describe a kinetically controlled crystallization process assisted by an oriented attachment (OA) mechanism based on a nonaqueous sol–gel synthetic method (specifically, the reaction of titanium(IV) chloride ($TiCl_4$) with *n*-octanol) to prepare re-crystallized anatase TiO_2 mesocrystals (single crystal). The kinetics study revealed a multi-step and hierarchical process controlled by OA, and a high resolution transmission electron microscopy (HRTEM) analysis clearly shows that the synthesized mesocrystal presents a truncated bipyramidal Wulff shape, indicating that its surface is dominated by {101} facets. This shape is developed during the recrystallization step. The material developed here displayed superior photocatalytic activity under visible light irradiation compared to TiO_2–P25 as a benchmarking.

Introduction

The development of new synthetic routes aiming to obtain nanocrystals and mesocrystals with controlled shapes and reactive surfaces is of great scientific and technological interest, especially for chemical and photochemical heterogeneous catalytic processes.[1–5] For instance, recently Shen and co-authors have demonstrated that the morphological control of Co_3O_4 was fundamental to improve the activity and stability of this oxide for CO oxidation.[4] Following the same trend, the development of other nanostructured metal oxide with controlled morphology (or facets exposed on the surface) must result in materials with superior activity and stability for chemical and photochemical reactions.[2]

The titanium(IV) oxide (TiO_2) in the anatase phase is a key functional material with interesting sensing, photocatalytic and photovoltaic[6] surface dependent properties. The TiO_2 anatase crystal is usually dominated by {101} facets, which present the lowest surface energy.[7] Considering other facets, theoretical studies have demonstrated the following sequence for surface relative energies: {101} < {100} < {001}. An inversion in the sequence position between the {101} and {100} facets can occur; *e.g.*, in oxygenated surfaces, {100} facets are mostly stable whereas under clear and hydrogenated conditions, {101} facets are more stable. However, the {001} has the highest energy facets. The surface relative energy variations can basically be explained by the different chemical compositions of the facets, resulting in diverse degrees of broken chemical bonds on the surface.

Recently, a breakthrough in the synthesis of anatase TiO_2 crystals with {001} facets was achieved by Lu and co-authors.[8] They reported the preparation of anatase microcrystals with surfaces formed preferentially by {001} facets. On the basis of first-principle quantum chemistry calculations, the strategy used by them was the reversal of the relative stability of the facets through the use of fluoride ions during the synthesis. The presence of fluoride ions favors the formation of high F–Ti bonding energy at the surface, leading to a decrease in the (001) surface energy, which results in more stability than the (101) surface. Then Zheng and co-workers used a similar approach to synthesize anatase TiO_2 nanosheets with exposed {001} facets and excellent photocatalytic performance.[9] The crystallization mechanism of the anatase with {001} exposed facets synthesized in hydrofluoric acid solution (under hydrothermal conditions) should be related to monomer-by-monomer assembly; *i.e.*, the attachment of ions/molecules to a primary nucleus. The fluorine ions must act as selective surface poisoning agents following a classical and thus predictable crystallization process. Ohtani and co-workers[10] also recently reported the formation of anatase TiO_2 with exposed {001} facets and high photocatalytic activity; however, they used a gas phase reaction process and $TiCl_4$ as a titanium precursor. The authors did not discuss the surface energy stabilization, but the presence of chloride can promote

[a]*Chemistry Department, Federal University of São Carlos, São Carlos, SP, 13656-905, Brazil. E-mail: derl@power.ufscar.br; Fax: +55 16 33615215; Tel: +55 16 33519567*

[b]*Brazilian Synchrotron Light Laboratory, Campinas, SP, 13083-970, Brazil. E-mail: antonio.ramirez@lnls.br; Fax: +55 19 35121004; Tel: +55 19 35183108*

[c]*Materials Engineering Department, Mechanical Engineering School, University of Campinas, Campinas, SP, 13083-860, Brazil*

† Electronic supplementary information (ESI) available: HRTEM images of the material synthesized with a magnetic stirrer (Fig. S1), XRD analysis of the material synthesized with a magnetic stirrer (Fig. S2) and EDS-TEM analysis showing the low chloride concentration of the material synthesized at 100 °C (40 h of treatment time) without a magnetic stirrer. See DOI: 10.1039/conr01016b

(001) surface stabilization following a mechanism similar to the mechanism reported by Lu and co-authors.[8]

An alternative route to process inorganic materials is through a kinetically controlled crystallization process driven by an oriented attachment (OA) growth mechanism.[11] In this non-classical crystallization process, the formation of a crystal controlled by monomer-by-monomer assembly is replaced by a process involving the spontaneous self-organization of adjacent nanocrystals to share a common crystallographic orientation and coalescence; *i.e.*, by the OA growth mechanism.[12] The number of materials obtained by the OA driven process is growing rapidly and has become an attractive form of processing anisotropic nanocrystals and mesocrystals.[12,13] The development of synthetic routes based on a non-classical crystallization process is particularly desired, because in this approach it is not necessary to use hydrofluoric acid which is extremely corrosive and a contact poison reagent. For instance, Niederberger's group synthesized anatase TiO_2 nanowires with a diameter of 3 nm and a length of several hundred nm formed by nanocrystals assembled along the [001] direction.[14] The initial anatase TiO_2 nanocrystal was synthesized in benzyl alcohol and the OA growth along the [001] direction was achieved by the selective desorption of multidentate ligands from the {001} facets.[14b]

Sol–gel routes based on complex aqueous chemistry or nonaqueous processes are suitable to obtain anatase TiO_2 nanocrystals.[15] In comparison with complex aqueous chemistry, nonaqueous processes offer the possibility for greater control of the reaction pathways on a molecular level, enabling the synthesis of nanomaterials with high crystallinity as well as with well-defined and uniform particle morphologies. The organic components strongly influence the composition, size, shape and surface properties of the inorganic product.

In this work, we propose a kinetically controlled crystallization process assisted by an OA mechanism, based on a non-aqueous sol–gel synthetic method to prepare anatase TiO_2 recrystallized mesocrystals with a truncated tetragonal bipyramidal Wulff shape. More specifically, we use the solvothermal reaction of titanium(IV) chloride ($TiCl_4$) with *n*-octanol ($CH_3(CH_2)_7OH$) under different kinetic conditions (*i.e.*, varying reaction times and concentrations) at 100 °C. Detailed HRTEM analysis of the growth process suggests a multi-step and hierarchical process. We also measured the photochemical activity of this exotic nanocrystal through the photocatalytic degradation of an organic dye (rhodamine B) under visible light irradiation. The word "recrystallization" is a general term used to describe a solid–solid transformation from a mesocrystal intermediate to a single crystal. In this context the meaning of "recrystallized mesocrystal" is equivalent to monocrystal and the term mesocrystal used in this manuscript denotes a mesocrystal intermediate, as suggested by Penn *et al.*[21b]

Experimental section

Materials

Titanium chloride ($TiCl_4$) (99.995%) and *n*-octanol (99%) were purchased from Aldrich and used as received. Tetrahydrofuran (THF) used during the washing procedures and rhodamine B (RhB) (both of ACS grade) were purchased from J. T. Baker (USA). The solvothermal treatment was performed in a sealed glass bottle under no stirring. Commercial grade, nanosized TiO_2 (Degussa P25) was used without further purification or treatment. Deionized water was used throughout the photocatalytic study.

Synthesis

The mixtures between the metal precursor and the solvent were made in a glove box under a controlled atmosphere. Titanium dioxide was synthesized following the non-aqueous sol–gel principle using 1-octanol (*n*-octanol) as the solvent.[15] $TiCl_4$ (18.2 mmol, 3.45 g) was slowly added dropwise into a glass vessel with octyl alcohol (40 ml) and homogenized at the end of the addition. After mixing and dissolution of the precursor, the reaction vessel was taken out of the glove box and heated to 100 °C for different times in a silicon oil bath with an immersed k-type thermocouple to control the temperature, although no further stirring was performed. A similar synthesis was performed with a lower (9.1 mmol in 40 ml of *n*-octanol) and a higher (36.4 mmol in 40 ml of *n*-octanol) $TiCl_4$ concentration, keeping the reaction time (80 h) and temperature (100 °C) constant.

Characterization

After a drying step, the resulting powder was used for X-ray diffraction (XRD) phase characterization using CuKα radiation (Rigaku D/MAX 2500 PC with a rotary anode operating at 150 kV and 40 mA). HRTEM images were obtained with a TECNAI F20 microscope operating at 200 kV with energy-dispersive X-ray spectroscopy (EDX). The specific surface area was measured using a BET surface area analyzer (Micrometrics, ASAP 2000). Samples were degassed under vacuum for 2 h at 150 °C prior to the BET analysis.

Photocatalytic activity measurements

The photocatalytic activity of the samples was evaluated through the decolorization of rhodamine B (RhB) in aqueous solution under visible light 150 W tungsten halogen lamp (the maximum light intensity centered at 640 nm with a wavelength window of 400 to 800 nm), which was kept at a fixed distance from the photo-reactor. The photo-reactor was made of a cylindrical glass vessel with a recycling water glass jacket coupled to a constant temperature water circulator. In this work, we used a different strategy to compare the photocatalytic activity between P25 and synthesized TiO_2, instead of standardizing the photodegradation measurements by weight. It was standardized by the surface area equivalent to 2 m^2 for each compound (according to the data provided by the BET measurement). The experiments were performed at 25 °C (±0.1°) as follows: 0.44 mmol (35 mg) of TiO_2 synthesized by a non-aqueous method was added into 100 ml of rhodamine-B solution (10^{-5} mol L^{-1}); 0.65 mmol (52 mg) of TiO_2–P25 was subjected to the same procedures. Before illumination, photocatalysts were not submitted to any previous treatment and then were dispersed in RhB solution under magnetic stirring for 30 minutes and were protected from any source of light. Then the solution was stirred and exposed to visible light irradiation. After irradiation for a designated time,

aliquots were taken from the irradiated reaction flask and submitted to centrifugation to separate TiO_2 particles. The RhB concentration was monitored by the absorbance value at the maximum peak (553 nm) by checking the absorbance during the photodegradation process using a Shimadzu 1501 UV-Vis spectrometer.

Results and discussion

Considering we are using a non-classical and non-predictable crystallization process, we conducted trial-and-error experiments to select better synthesis conditions. The selection of the alcohol to be used in the nonaqueous sol–gel synthesis is a determinant parameter in our approach because different kinds of alcohols lead to different phases (anatase and rutile) and the morphology of the TiO_2 nanocrystal.[15c] Furthermore, if we use a kinetically controlled crystallization process, we need to provide an appropriate physical–chemical environment that allows the development of the OA mechanism during the synthesis. In principle, there are two possible ways to achieve the OA mechanism: (1) an effective collision of particles with the same crystallographic orientation; and (2) coalescence induced by nanocrystal rotation in a weakly coagulated colloid.[16] The second way is more appropriate in a growth process controlled by the self-assembly of nanoparticles. In addition, the choice of whether to stir during the synthesis is also important because in a static condition (without stirring), the OA process controlled by nanocrystal rotation must be favorable for the self-assembly of nanoparticles. Considering all these arguments, we carried out a synthesis in a static condition (without stirring), using *n*-octanol as the solvent under 100 °C varying the reaction time.

Since we used a glass reactor, it was possible to follow the reaction by visual inspection. At 100 °C, the initial transparent solution becomes opaque, showing a white color after 8 hours of reaction. XRD patterns of the nanocrystals synthesized in different reaction times (Fig. 1) indicate the crystallization of anatase nanocrystals without a preferential growth direction. By increasing the reaction time, we observed a well defined XRD pattern for the anatase phase as well as traces of a rutile phase in a concentration lower than 5%. Li and co-authors[17] reported the synthesis of a rutile phase with fiber morphology but no anatase phase for the reaction of $TiCl_4$ with *n*-octanol at 100 °C. We only observed the extensive formation of a rutile phase with fiber morphology when we used a magnetic stirrer during the synthesis process (see Fig. S1 and S2 in the ESI†). Considering that the reaction between the $TiCl_4$ and *n*-octanol is mainly controlled by the ether elimination mechanism, it is postulated that the presence of a rutile phase is related to the retention of hydrogen chloride (HCl) in the reaction system.[15] In our experiment, the synthesis of anatase nanocrystals with very low concentrations of the rutile phase can be attributed to the static reaction condition used; however, how this condition avoided the interaction between the HCl and the crystal surface is not clear. We believe that the presence of *n*-octanol attached to the surface negates the interaction between HCl and the anatase nanocrystal. This hypothesis is consistent with the very low chloride content measured by EDS-TEM analysis in the anatase nanocrystal (see Fig. S3 in the ESI†). The crystallite size measurement, considering the Scherrer equation and the (101) plane of the Anatase phase, of the nanocrystals synthesized in different reaction times showed a size of 12 nm for the reaction time of 8 h and a size of 23 nm for material synthesized during 48 h.

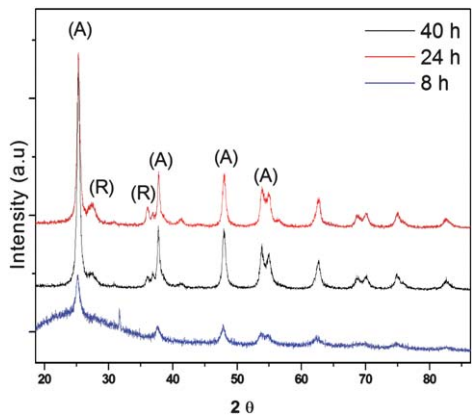

Fig. 1 XRD pattern of the material synthesized at 100 °C at different treatment times (18.2 mmol $TiCl_4$ in 40 ml of *n*-octanol). (A) = Anatase phase and (R) = rutile phase.

To analyze the particle morphology of the material synthesized at different times, we performed a HRTEM characterization. Fig. 2 shows low and high magnification HRTEM images of the material synthesized at 8 h, 24 h and 40 h. The low magnification HRTEM image of the material synthesized at 8 h (Fig. 2a) shows the presence of larger agglomerates. It is interesting to observe that the large agglomerate is formed by smaller agglomerates with a square-like morphology, and a size in the range of 25–30 nm. A closer analysis of the smallest agglomerate (see Fig. 2b) shows that it is formed by primary nanocrystals in a size ranging from 3–5 nm with similar crystallographic orientation. The common orientation among nanocrystals can easily be visualized in the reconstructed lattice image of Fig. 2b (inset) where we can observe a boundary as well as a region with perfect and imperfect attachments and alignments between particles. The aggregations of several nanocrystals with similar crystallographic orientations forming larger agglomerates as well as the presence of defects are strong evidence that the OA process is the predominant nanocrystal growth mechanism.[18] The HRTEM analysis suggests that the crystallite size measured by XRD (12 nm) is related to the size of the agglomerates formed by several nanocrystals with similar crystallographic orientations, and not related to the size of the primary nanoparticle.

By increasing the reaction time, we can observe in Fig. 2c and d a better assembly of the primary nanocrystals forming denser agglomerates. Analyses of the high magnification HRTEM image (Fig. 2d) provide strong evidence for the bi- and tri-dimensional attachment between the nanocrystals. The fast Fourier transform (FFT) of the region delimited by the white square of Fig. 2d shows reflections typical of a single-crystal oriented along the [0$\bar{1}$0] zone axis as illustrated in the inset of Fig. 2d. This analysis confirmed the formation of common orientation among nanocrystals, forming larger agglomerates with single crystal characteristics (from the crystallographic point of view), *i.e.*, a mesocrystal. After 40 hours of reaction time (see Fig. 2e and f), we observed the formation of agglomerates with well-defined shapes and very low porosity. Actually, the

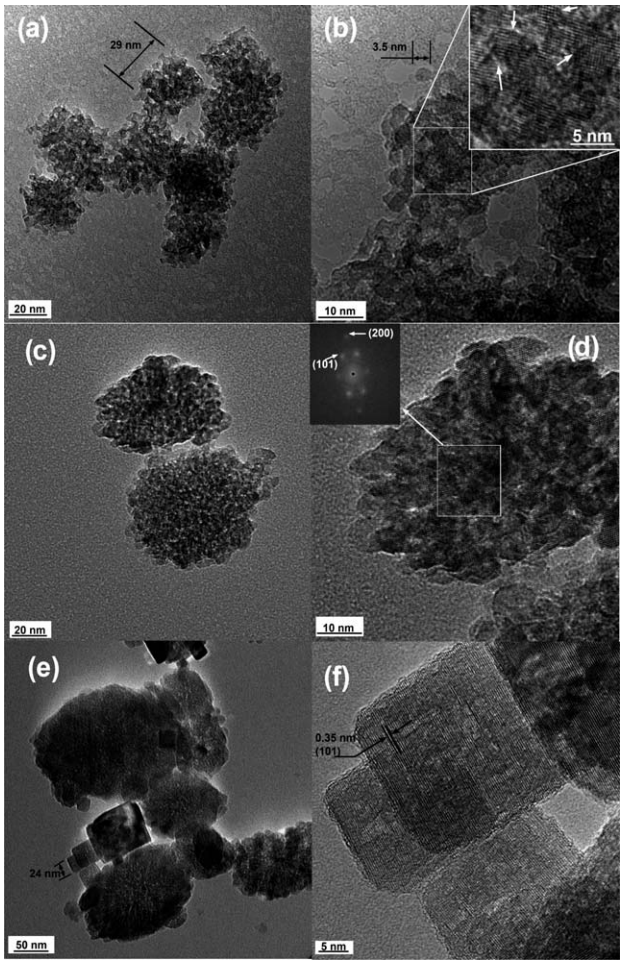

Fig. 2 Low and high magnification HRTEM images of the material synthesized during: (a) and (b) 8 h; (c) and (d) 24 h; (e) and (f) 40 h. The inset in Fig. 2b shows a reconstructed lattice image. The inset in Fig. 2d shows a FFT of the region delimited by the white square.

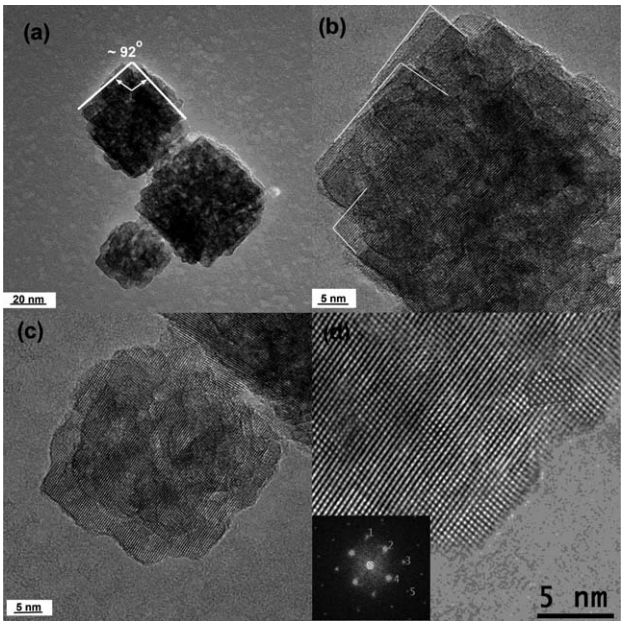

Fig. 3 HRTEM images of the material synthesized at 100 °C during 40 h. (a) Low magnification HRTEM image; and (b)–(d) high magnification HRTEM images. The insets in (d) show a FFT analysis (spots: #1 = (110), #2, 4 = (101), #3 = (112), #5 = (202)) and a multislice simulated HRTEM image of the rectangular black region.

boundary among the primary nanocrystals is no longer observed, indicating the occurrence of a self-recrystallization process associated to grain boundary mobility and elimination.[13] The agglomerates with well-defined shapes and very low porosity in fact are recrystallized mesocrystals (single crystals). We also observed the presence of recrystallized mesocrystal of several sizes, ranging from 20 nm to agglomerates larger than 100 nm. This wide range of sizes suggests a hierarchical growth process where the smaller agglomerates interact among themselves, resulting in a larger mesocrystal.

The hierarchical growth process is supported by the HRTEM images displayed in Fig. 3. In the low magnification HRTEM image of Fig. 3a, the interaction among three recrystallized mesocrystals with a well-defined boundary among them is displayed. We clearly observe that each mesocrystal is formed by the self-assembly of oriented clusters of nanocrystals (Fig. 3b) and that the boundary between the mesocrystals shares a common crystallographic orientation (Fig. 3c). Fig. 3d shows a high magnification HRTEM image where a well recrystallized mesocrystal can be observed. The FFT of this image (inset) shows a reflection typical of a single-crystal oriented along the [111] zone axis.

The rectangular black region indicated in Fig. 3d compares the multislice simulated HRTEM image with the experimental image. The good agreement between the images confirms the zone axis orientation indicated by FFT analysis.

The dependence of the size and morphology with the treatment time indicates a kinetic growth process controlled mainly by the OA mechanism. This kinetic growth process is also supported by the growth and morphology dependence upon the titanium precursor concentration. At low concentrations (Fig. 4a), we observed agglomeration morphology similar to the agglomeration morphology reported for shorter treatment times (see Fig. 2a and b) with the predominance of the OA growth mechanism (see the inset in Fig. 4a). For high concentrations, a recrystallized mesocrystal is observed (Fig. 4b and the inset). This result indicates the equivalence between the time and concentration for morphology development.

The crystal shape analysis can supply additional information about the growth process. Looking at the crystal morphology by TEM, we can identify faceted crystals with several geometries (see Fig. 3 and 4). In a first analysis, these different geometries can indicate crystals with varying morphologies. However, if we consider the truncated tetragonal bipyramidal Wulff shape predicted for the anatase TiO_2 phase, the bi-dimensional projection in different zone axes results in objects with alternate geometries (see Fig. 5). Since the TEM image is a bi-dimensional projection of a three-dimensional object, we can suppose that the different morphologies observed are in fact related to the projection of the truncated bipyramid in different zone axes. For the TEM image analysis, we can easily identify projections of the truncated bipyramid in different zone axes. For instance, Fig. 3d shows the FFT of the image with reflections typical of a single-crystal oriented along the [111] zone axis, confirming the square-like

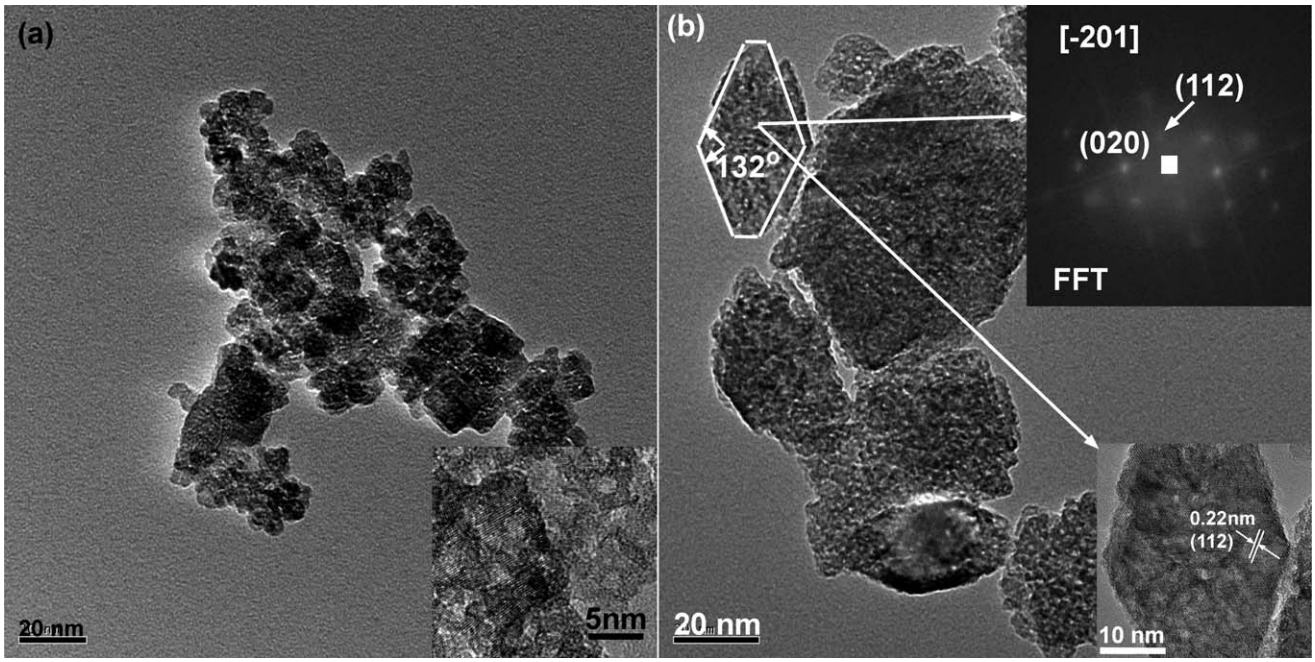

Fig. 4 HRTEM images of the material synthesized at 100 °C during 40 h. (a) Lower $TiCl_4$ concentration (9.1 mmol in 40 ml of *n*-octanol). The inset shows a reconstructed lattice image. (b) Higher $TiCl_4$ concentration (36.4 mmol in 40 ml of *n*-octanol). The insets show a high magnification HRTEM image and a FFT analysis of the region indicated by the white arrows.

morphology predicted by the projection of the truncated bipyramid in this direction. In the same way, Fig. 4b shows a FFT analysis with reflections typical of a single-crystal oriented along the [$\bar{2}$01] zone axis. The geometric shape observed for the recrystallized mesocrystal (see the mesocrystal highlighted by the white line in Fig. 4b) is also consistent with the predicted geometry originating from the projection of the truncated bipyramid along the [$\bar{2}$01] direction. The above analysis clearly shows the synthesized recrystallized anatase mesocrystals present a truncated bipyramidal Wulff shape, indicating that its surface is dominated by {101} facets. The observation of the Wulff shape for the recrystallized mesocrystal (single crystal) indicates that the equilibrium shape dictated by the minimization of surface energy is an important argument and must be taken into account to explain the growth mechanism.

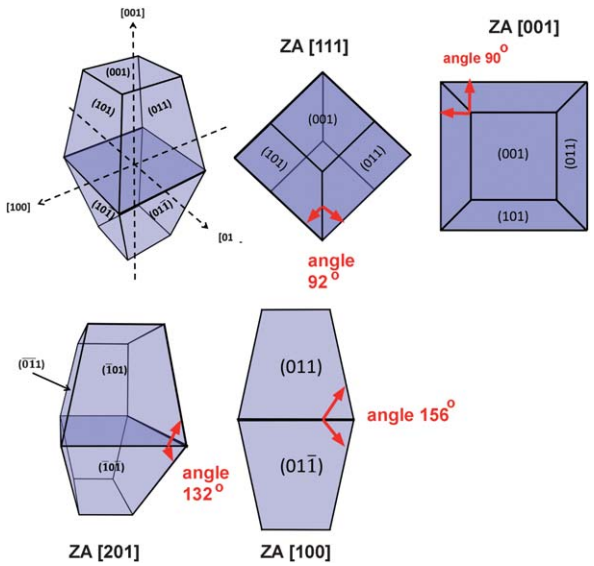

Fig. 5 The truncated tetragonal bipyramidal Wulff shape predicted for the anatase TiO_2 phase and the bi-dimensional projection of this object in different zone axes.

Apparently, here we have a contradiction between the observation of a kinetic growth process controlled by OA and the recrystallized mesocrystal shape dominated by thermodynamic arguments. However, we believe that this contradiction does not exist because we are describing a multi-step and hierarchical process where several phenomena occurred. In a didactical way, we can propose that the process starts with the nucleation and growth of anatase nanocrystals with a mean size around 3 nm. In the semi-coagulated state of the reaction medium, an attractive interaction between the nanocrystals must occur, resulting in agglomerates formed by the ordered assembly of the nanoparticles; *i.e.*, by the OA process (second step). In a third step, the agglomerates start to interact, resulting in larger and denser agglomerates with coherent crystallographic interfaces. The origin of the attractive interaction between nanoparticles (second stage) and agglomerates (third stage) is not clear; however, it can be associated with the presence of dipoles in the nanoparticles and agglomerates[19] or even a structural interaction promoted by the selective desorption process of the organic compounds attached to the nanoparticle surface.[14b,20] The fourth and final step is related to the self-recrystallization process of the mesocrystal. It is well documented in the literature that after the recrystallization step, the material grown by OA presents a defined shape.[21] Thus, we believe that the final shape of the crystals observed in this work is developed mainly in this last step.

A typical characteristic of the recrystallization process is that any movement (migration) of atoms or nanocrystals in the phases is hampered. Consequently, elastic deformation developed during the transformation process should be taken into account. In the self-recrystallization process reported here, a transformation of a mesocrystal to a single crystal occurs. The change in free energy (ΔG) at the transformation of the new single crystal can be described as:

$$\Delta G = -\Delta G' v + \Sigma \gamma_{ss} S + \Phi_{def} \quad (1)$$

where $\Delta G'$ is the change in the Gibbs free energy G' of the initial state (mesocrystal) and final (recrystallized mesocrystal or single crystal) transformation, v is the volume, γ_{ss} and S are specific surface energy and areas of interfaces (grain boundaries) respectively, and Φ_{def} is the term of the elastic deformation energy. We propose that the second and the elastic energy terms determine the final crystal morphology and that the shape dictated by the minimization of surface energy is mainly controlled by the change of the interface energy (the second term of eqn (1)). As a result of the limited mobility of the atoms or nanocrystals in the solid phase, cooperative movements of atoms should be considered to explain the grain boundary migration at low temperature. These cooperative movements of atoms with or without the presence of relaxation process lead to some specific mass transportation mechanism across the grain boundary (not identified as yet).

The combination of high crystallinity and high surface area of the recrystallized mesocrystal described in this work can be advantageous for photocatalytic application compared to unordered nanocrystalline aggregate. Thus we decided to evaluate its photocatalytic performance. The degradation rate of the heterogeneous photocatalytic reaction of the recrystallized anatase mesocrystal synthesized with a reaction time of 40 h was monitored by the decolorization of rhodamine-B (RhB) under visible light. It is worth pointing out that the photocatalytic experiment under consideration is a photo-activated process, where the dye (RhB) adsorbed on the metal oxide surface provides the injected electrons to the conduction band of TiO_2, which contributes to yield reactive species such as anions (O_2^-) and radicals ($^{\bullet}OH$), as showed by Serpone *et al.*[22] The photolysis of RhB under visible light irradiation in the absence of a catalyst is negligible, the capability of the RhB decolorization per unit of the BET surface area as a function of the time at constant temperature of the material synthesized in this work (a BET surface area of 56.7 $m^2 g^{-1}$ and a very low content of mesoporous analyzed by the BJH method) was compared with TiO_2–P25 as a reference (a BET surface area of 38.5 $m^2 g^{-1}$ and a very low mesoporous content analyzed by the BJH method); the results are shown in Fig. 6. The materials synthesized here showed faster decolorization kinetics when compared with the reference material with a corresponding half-life of 140 minutes compared with 310 minutes for TiO_2–P25. The results clearly demonstrate substantial enhanced photoreactivity under visible radiation of the recrystallized anatase mesocrystal, which is not related to the surface area effect (since the photodegradation measurements were standardized by the surface area of both titania compounds) or exposure of a specific crystallographic facet, and is attributable to the different physical–chemistry nature of the recrystallized mesocrystal surface (a higher number of activity sites for this photocatalytic reaction).

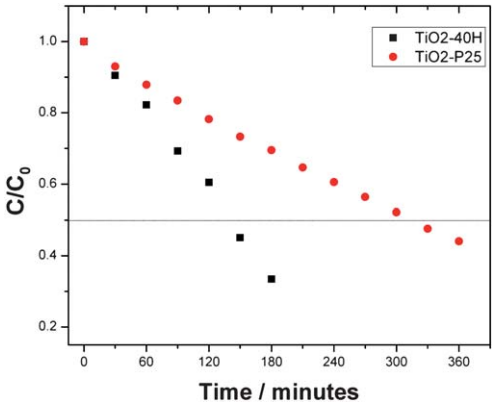

Fig. 6 RhB concentration as a function of the photo-degradation reaction time over recrystallized anatase mesocrystals synthesized in this work (TiO_2–4Oh) and TiO_2–P25 nanoparticles. The dotted line indicates the half-life of the initial concentration.

Conclusions

We present here a novel solvothermal synthesis approach for preparation of recrystallized anatase TiO_2 mesocrystals based on a kinetically controlled growth mechanism assisted by the OA process using a non-aqueous sol–gel process, *i.e.*, a chemical process based on the reaction of titanium(IV) chloride ($TiCl_4$) with *n*-octanol. The kinetics study describes a multi-step and hierarchical process controlled by OA. The HRTEM analysis clearly shows the synthesized recrystallized anatase mesocrystal presents a truncated bipyramidal Wulff shape, indicating that its surface is dominated by {101} facets. The final shape of the mesocrystal is defined during the self-recrystallization step. The material developed here displayed superior photoreactivity for the RhB degradation under visible irradiation light as compared to P25 as a benchmarking material. The concepts here developed can be applied in the synthesis of several mesocrystals, becoming a work of general interest.

Acknowledgements

The financial support of FAPESP (Projects 98/14324-0), FINEP, CNPq and CAPES (all Brazilian agencies) is gratefully acknowledged.

References

1 A. Seyed-Razavi, I. K. Snook and A. S. Barnard, *J. Mater. Chem.*, 2010, **20**, 416–421.
2 G. Liu, L. Wang, H. G. Yang, H.-M. Cheng and G. Q. Lu, *J. Mater. Chem.*, 2010, **20**, 831–843.
3 A. Halder, P. Kundu, B. Viswanath and N. Ravishankar, *J. Mater. Chem.*, 2010, **20**, 4763–4772.
4 X. Xie, Y. Li, Z.-Q. Liu, M. Haruta and W. Shen, *Nature*, 2009, **458**, 746–749.
5 X. Xie and W. Shen, *Nanoscale*, 2009, **1**, 50–60.
6 (*a*) M. Ferroni, M. C. Carotta, V. Guidi, G. Martinelli, F. Ronconi, M. Sacerdoti and E. Traversa, *Sens. Actuators, B*, 2001, **77**, 162–166; (*b*) Z. B. Zhang, C. C. Wang, R. Zakaria and J. Y. Ying, *J. Phys. Chem. B*, 1998, **102**, 10871–10878; (*c*) A. Hagfeldt and M. Graetzel, *Acc. Chem. Res.*, 2000, **33**, 269–277.
7 (*a*) M. Lazzeri, A. Vittadini and A. Selloni, *Phys. Rev. B: Condens. Matter Mater. Phys.*, 2002, **65**, 119901; (*b*) U. Diebold, *Surf. Sci. Rep.*, 2003, **48**, 53–229.
8 (*a*) H. G. Yang, C. H. Sun, S. Z. Qiao, J. Zou, G. Liu, S. C. Smith, H. M. Cheng and G. Q. Lu, *Nature*, 2008, **453**, 638; (*b*)

H. G. Yang, G. Liu, S. Z. Qiao, C. H. Sun, Y. G. Jin, S. C. Smith, J. Zou, H. M. Cheng and G. Q. Lu, *J. Am. Chem. Soc.*, 2009, **131**, 4078–4083.
9 X. Han, Q. Kuang, M. Jin, Z. Xie and L. Zheng, *J. Am. Chem. Soc.*, 2009, **131**, 3152–3153.
10 F. Amano, O.-O. Prieto-Mahaney, Y. Terada, T. Yasumoto, T. Shibayama and B. Ohtani, *Chem. Mater.*, 2009, **21**, 2601–2603.
11 R.-Q. Song and H. Colfen, *Adv. Mater.*, 2009, **21**, 1–30.
12 M. Niederberger and H. Colfen, *Phys. Chem. Chem. Phys.*, 2006, **8**, 3271–3287.
13 J. Zhang, F. Huang and Z. Lin, *Nanoscale*, 2010, **2**, 18–34.
14 (*a*) J. Polleux, N. Pinna, M. Antonietti and M. Niederberger, *Adv. Mater.*, 2004, **16**, 436–439; (*b*) J. Polleux, N. Pinna, M. Antonietti, C. Hess, H. Wild, R. Schlogl and M. Niederberger, *Chem.–Eur. J.*, 2005, **11**, 3541–3551.
15 (*a*) A. Vioux, *Chem. Mater.*, 1997, **9**, 2292–2299; (*b*) P. H. Mutin and A. Vioux, *Chem. Mater.*, 2009, **21**, 582–596; (*c*) G. Garnweitner and M. Niederberger, *J. Mater. Chem.*, 2008, **18**, 1171–1182.
16 (*a*) E. J. H. Lee, C. Ribeiro, E. Longo and E. R. Leite, *J. Phys. Chem. B*, 2005, **109**, 20842; (*b*) H. Colfen and M. Antonietti, *Mesocrystals and Nonclassical Crystallization*, John Wiley & Sons, Hoboken, 2008, p. 84.
17 C. Wang, Z.-X. Deng, G. Zhang, S. Fan and Y. Li, *Powder Technol.*, 2002, **125**, 39–44.
18 (*a*) R. L. Penn and J. F. Banfield, *Geochim. Cosmochim. Acta*, 1999, **63**, 1549–1557; (*b*) R. L. Penn and J. F. Banfield, *Science*, 1998, **281**, 969–971.
19 Recently Fichthorn and Alimohammadi showed that asymmetric particles (which mimic the Wulff shape of the anatase) show a strong dipole moment. For instance, an anatase bipyramid truncated in one of the {001} facets results in a dipole moment of $\mu \cong 35$ D: M. Alimohammadi and K. A. Fichthorn, *Nano Lett.*, 2009, **12**, 4198–4203.
20 J. A. Lewis, *J. Am. Ceram. Soc.*, 2000, **83**, 2341–2359.
21 (*a*) Z. Y. Tang, N. A. Kotov and M. Giersig, *Science*, 2002, **297**, 237–240; (*b*) V. M. Yuwono, N. D. Burrows, J. A. Soltis and R. L. Penn, *J. Am. Chem. Soc.*, 2010, **132**, 2163–2165; (*c*) D. Schwahn, Y. R. Ma and H. Colfen, *J. Phys. Chem. C*, 2007, **111**, 3224–3227.
22 T. Wu, G. Liu, J. Zhao, H. Hidaka and N. Serpone, *J. Phys. Chem. B*, 1998, **102**, 5845–5851.

